Title

Effect of Initial State of Lithium on the Propensity for Dendrite Formation: A Theoretical Study

Journal

Journal of The Electrochemical Society, 164(2)

ISSN

0013-4651

Authors

Barai, Pallab
Higa, Kenneth
Srinivasan, Venkat

Publication Date

2017

DOI

10.1149/2.0661702jes

Effect of initial state of lithium on the propensity for dendrite formation: A theoretical study

Pallab Barai, Kenneth Higa, Venkat Srinivasan*

Energy Storage and Distributed Resources Division,

Lawrence Berkeley National Laboratory, Berkeley, CA, 94720

Submitted to

Journal of The Electrochemical Society

October, 2016

*Corresponding author: Dr. Venkat Srinivasan (email: vsrinivasan@lbl.gov)

Abstract

Mechanical constraints have been widely used experimentally to prevent the growth of dendrites within lithium metal. The only article known to the authors that tries to theoretically understand how mechanical forces prevent dendrite growth was published by Monroe and Newman (*Journal of the Electrochemical Society*, **150** (10) A1377 – A1384 (2005)). Based on the assumption that surface tension prevents the growth of interfacial roughness, Monroe and Newman considered *pre-stressed* conditions of the lithium electrodes. This scenario indicates that prevention of dendrite growth by mechanical means is only possible by using electrolytes with shear modulus at least two times larger than that of lithium metal. A different scenario of *relaxed* lithium metal (without any pre-existing surface stresses) has been considered in the present analysis. Deposition of lithium due to electrochemical reaction at the lithium/electrolyte interface induces compressive stress at the electrode, the electrolyte, and the newly deposited lithium metal. Present simulations indicate that during operation at low current densities, the scenario of *relaxed* lithium leads to no dendrites. Rather, the present study points to the importance of including the effect of current distribution to accurately capture the mechanical forces needed to prevent dendrite growth.

Keywords: *dendrite growth, lithium metal anode, mechanical stress* and *effective exchange current density*.

Introduction

Due to its extremely negative potential with respect to standard hydrogen electrode (-3.04V) and very high theoretical specific capacity (3870mAh/g), lithium metal is considered the ultimate anode material for lithium-based batteries. The potential of lithium to produce high-energy density batteries was recognized very early in the 1970s [1-3]. However, formation and growth of dendrites during the charge process, and subsequent internal short-circuit is the biggest obstacle faced by lithium metal as the anode material[4, 5]. Low coulombic efficiency due to the formation of “dead” lithium and excessive side reactions has also been a major drawback of lithium metal anodes[6-8]. Presently, it is well accepted in the scientific community that mossy lithium deposit is observed under low current density and dendritic protrusion occurs during high current density operations[9].

In the past few decades, significant amount of research has been devoted to experimentally visualize the growth of dendrites and understand the mechanism behind their formation[5, 10]. Along with in-situ scanning/transmission electron microscopy (SEM/TEM) imaging techniques[11-14], electrochemical impedance spectroscopy (EIS) [15, 16] and nuclear magnetic resonance (NMR)[15, 17] images have also been used to predict the location and morphology of the dendritic protrusion. Optimization of the electrolyte solvent, salt and several additives were conducted to form a stable SEI layer, which was initially expected to mitigate dendrite growth[18-20]. Low coulombic efficiency and weak mechanical strength are the major drawbacks why the SEI layers are unable to completely eliminate the dendrite formation[21]. Stiff mechanical barriers in the form of nitrogen and sulfur co-doped graphene oxide[22] and porous ceramic

layers[23] have been successfully used to mitigate the formation of dendritic protrusions. However, relatively soft ionic liquids[15] and polymer electrolytes[24] have also displayed significant potential to reduce the growth of dendrites. There also exist experimental evidence of reduced dendrite growth under externally applied pressure[25, 26].

To understand the mechanism behind the growth of dendritic protrusions, the first theoretical model was developed by Barton and Bockris, where they presented a diffusion controlled mechanism for the propagation of dendrites[27]. Later on Diggle et al. incorporated the effect of surface energy to prevent the infinite thinning of the dendrites[28]. Chazalviel developed a model for the initiation of dendritic protrusions based on the hypothesis of lack of electric neutrality, which is only satisfied beyond the limiting current densities[29, 30]. Butler-Volmer reaction kinetics and diffusion controlled growth of dendrite tips were modeled by Monroe and Newman[4]. The surface energy term was able to only slow down the growth of dendritic protrusions. More recently, based on thermodynamic energy considerations, a critical radius of dendrites has been proposed, beyond which growth of the protrusion occurs[31]. Any lithium nucleation smaller than this critical radius becomes unstable and gets dissolved. The value of the critical radius also depends on the applied overpotential. Following this energy based theoretical premise, a phase field model has been developed to predict the growth and morphology of dendritic protrusions[32]. Other phase field based dendrite growth models demonstrate the competition between diffusion and migration in determining the shape and morphology of these protruding structures[33, 34]. Coarse-

grain Monte-Carlo based stochastic simulations revealed that pulse charging can be beneficial in preventing dendrite growth as compared to constant charging protocols[35].

All the theoretical models discussed until now considered the effects of reaction kinetics, migration/diffusion induced transport and surface tension on the growth mechanism of dendrites. The effect of externally applied pressure and mechanical stress due to interaction with adjacent components (such as, SEI and electrolytes) are less understood. However, it has been hypothesized, based on experimental evidence, that rupture in the SEI layer as well as externally applied pressure significantly affects the formation of dendrites[21, 25]. The first efforts to understand how the mechanically applied hydrostatic and deviatoric stresses impact the growth of dendrites were initiated by Monroe and Newman[36, 37]. They modified the Butler-Volmer equation by incorporating the mechanical-stress-induced change in electrochemical potential of the electrons located within the lithium metal electrode[36]. Applying this to a small sinusoidal perturbation at the lithium/electrolyte interface (see Eq. 13 in Ref. [37]), representing a dendrite nucleation site, they calculated the exchange current density at the peak compared to the valley of the deposit. Monroe and Newman assumed that this initial perturbation places the lithium metal into a tensile *pre-stressed* state[37], with the lithium metal initially under tensile stress at the peak, and the electrolyte initially experiencing compression. During lithium deposition, compressive forces act within the electrolyte/separator assembly. A schematic diagram of this scenario is presented in Figure 1(a-c), which we will characterize as Scenario A or the *pre-stressed* scenario. Monroe and Newman found that preventing the dendritic protrusion from growing would require the elastic modulus of the electrolyte/separator to be 1.8 times larger than that of

lithium metal. Surface forces showed negligible impact in dendrite propagation even under very low modulus of the electrolyte/separator (see Fig. 5 in Ref. [37]).

In the present article we retain the same interfacial shape of the dendrite nucleation site but hypothesize that the lithium metal is initially in a stress-free *relaxed* state. The computational model developed by Monroe and Newman to analyze the *pre-stressed* lithium[36, 37], is extended to predict the early dendrite growth behavior from this initially *relaxed* state. A schematic diagram of this scenario is presented in Figure 1(d-f), which we will characterize as Scenario B or the *relaxed* scenario. During operation due to the electrochemical reaction, new lithium deposits at the metal-electrolyte interface. To accommodate this newly deposited lithium, both the lithium metal electrode and the electrolyte (either liquid or polymer) pushes backward, which gives rise to compressive stress. Similarly, the lithium deposit also experiences compressive force from the surrounding electrode and electrolyte. Hence, lithium metal, electrolyte and the new deposits, all experience compression. This scenario is different from the *pre-stressed* condition considered by Monroe and Newman, where the lithium metal was considered to be under tension[37]. The amount of deformation experienced by the lithium metal and the electrolyte depends on their individual elastic modulus. If the electrolyte is much softer than the lithium metal, majority of the deformation is accommodated by the electrolyte. Less mechanical stress should evolve in this case. Otherwise, for equal elastic modulus of lithium metal and electrolyte, both the phases deform in equivalent amount. We hypothesize that in the *relaxed* scenario (adopted in the present research), presence of compressive stresses within lithium will lead to significantly different distribution of exchange current density.

In this article, a quantitative analysis will be conducted to contrast the predictions from the *pre-stressed* scenario to that of the *relaxed* scenario with the aim of identifying which approach more closely describes the experimental literature. In order to keep the analysis focused on the initial state of the lithium, the study here will focus on extremely small current densities, wherein the impact of transport and kinetics on dendrite growth can be ignored. The stability criterion proposed by Monroe and Newman[37] will be reanalyzed based on the two scenario. The effect of surface tension on the exchange current density will be recalculated for the *pre-stressed* and *relaxed* initial state of lithium metal. In general, the impact of mechanical stress on the lithium nucleation and growth process will be elucidated here.

Methodology

During lithium deposition on an electrode (cathodic reaction), experimental evidence suggests that mossy deposits occur at lower current densities, and dendrites grow only during high current density operation [25]. It has been proposed that usage of a separator and/or electrolyte with elastic modulus double in magnitude than that of lithium can definitely prevent dendrite growth[37]. In their theoretical analysis, Monroe and Newman assumed lithium metal to be in a *pre-stressed* state (see Figure 1(a-c)) [37]. In the present study, we revisit the initial state of lithium metal and hypothesize it to be in a *relaxed* condition (as compared to *pre-stressed* configuration reported earlier), see Figure 1(d-f) for a schematic representation of the present scenario. The technique presented in Monroe and Newman[36, 37] has been extended here for analyzing the *relaxed* state of lithium. In order to keep the analysis similar to them, lithium deposition at extremely low

rates of current density will be analyzed, wherein the potential and lithium concentration distribution have little effect on dendrite growth process. The impact from mechanical stress and local surface curvature on the effective exchange current density (defined later) will be reported here. Impact of the two different scenarios, *pre-stressed* lithium (Scenario: A) and *relaxed* lithium (Scenario: B), on the dendrite growth process will be analyzed using theoretical/computational techniques.

In the cathodic reaction of lithium deposition, lithium-ions from the electrolyte combine with electrons and deposit as lithium metal, which can be written as:

$$Li^{+} + e^{-} \rightarrow Li\downarrow \tag{1}$$

Non-uniform deposition of the lithium metal leads to unevenness at the electrode and electrolyte interface. Under high current density, these variations lead to growth of dendrites. However, propagation of dendritic protrusions can be prevented by application of mechanical stress. To estimate the hydrostatic and deviatoric stress distributions around the deposit, the quasistatic equilibrium equation should be solved:

$$\vec{\nabla} \cdot \underset{\approx}{\sigma} = 0 \tag{2}$$

Here, $\vec{\nabla}$ indicates the gradient operator and $\underset{\approx}{\sigma}$ is the second order stress tensor. In this article, the vector/tensor and indicial notations have been used interchangeably. Also the

body force and inertia terms have been neglected. The total stress tensor $\left(\sigma_{ij}\right)$ has been divided into deviatoric $\left(s_{ij}\right)$ and hydrostatic $\left(\sigma_{kk}\right)$ components.

$$\sigma_{ij} = s_{ij} + \frac{1}{3}\sigma_{kk}\delta_{ij} \tag{3}$$

Here, δ_{ij} indicates the Kronecker delta function. Under the assumption of small strain $\left(\epsilon_{ij}\right)$, the strain-displacement kinematic relation is given as:

$$\epsilon_{ij} = \frac{1}{2}\left(\frac{\partial u_i}{\partial x_j} + \frac{\partial u_j}{\partial x_i}\right) \tag{4}$$

Here, $\vec{u}$ and $\vec{x}$ represents the displacement and position vector, respectively. The stress-strain constitutive relations are given in terms of the shear modulus $\left(G\right)$ and Poisson's ratio $\left(\nu\right)$:

$$\sigma_{ij} = 2G\epsilon_{ij} + \frac{2\nu G}{1-2\nu}\epsilon_{kk}\delta_{ij} \tag{5}$$

The above-mentioned set of Eqs (2-5) has been solved using the finite element method (FEM). Since the initial yield strength of lithium metal is around 0.8MPa[38], plastic deformation in lithium anode is inevitable. However, in the present analysis only the elastic stress-strain constitutive relations have been used to directly compare our results with that obtained by Monroe and Newman[37]. Details of the solution procedure are provided in the Appendix section.

Difference between the initially *pre-stressed* (scenario A) and *relaxed* (scenario B) lithium are modeled by applying different boundary conditions at the lithium-electrolyte interface. Figure 2(a-b) demonstrates the computational mesh adopted to estimate the evolution of stress experienced by the *pre-stressed* scenario. Zero displacement is applied at the two boundaries extremely far away from the lithium-electrolyte interface (see Figure 2(a)). Initially the lithium and electrolyte are flat:

$$\vec{u} = 0 \quad \textit{at the top of electrolyte and bottom of lithium.} \tag{6}$$

At the lithium-electrolyte interface, a sinusoidal displacement is applied along the z-direction with amplitude $H = 4nm$ and frequency $\omega = 10^8 Hz$ (see Figure 2(b)) [37].

$$u_{z,interface}(x) = H\cos(\omega x) \tag{7}$$

The dendritic protrusion within the lithium metal is generated by pulling the interface upward according to a displacement prescribes boundary condition. This induces tensile stress in lithium and compression at the electrolyte. Pre-existing tension within the lithium metal at the lithium-electrolyte interface can be attributed to surface stresses

induced by manufacturing processes. Periodic boundary condition has been applied at the left and right boundaries of the computational domain.

The second scenario considers that the lithium metal is initially in a *relaxed* state (shown in Figure 1(d)). Deposition of lithium metal at the electrode/electrolyte interface due to electrochemical reduction would lead to generation of a new phase, which is separate from both electrode and electrolyte. This newly deposited lithium (due to electrochemical reactions) induces compressive stress at the lithium electrode, electrolyte and the new lithium phase itself (Figure (e-f)). Direct computational modeling of this new lithium phase can be accomplished by using "phase-field" based methodologies, which is out of scope of the present analysis. In order to simulate this phenomenon, the following steps have been implemented in the computational scheme:

1. Take a piece of flat lithium and fix the bottom according to Eq. (6).
2. Apply sinusoidal displacement at the top of lithium according to Eq. (7). Obtain the equilibrium displacement of the mesh. Relax all the stresses that act within the lithium metal due to induced displacement (see Figure 2(c)). The new position will be taken as "zero displacement" configuration to which future displacements are referenced.
3. Push the electrolyte phase from the top of the lithium metal, until the entire electrolyte comes in contact with the lithium metal (see Figure 2(d)) (please refer to the next paragraph for details regarding the contact modeling procedure).

This downward movement of the electrolyte induces compressive stress on the lithium metal as well as the electrolyte. This stress condition is very similar to that observed in scenario B (demonstrated by Figure 1(e)). Figures 2(c) and 2(d) represent the initial and final computational mesh, respectively, adopted to estimate the evolution of stress

according to the *relaxed* scenario B. On a different note, this process of attaching the electrolyte with the electrode also mimics the cell assembly with a piece of lithium without any residual stresses but which has a slightly flawed surface.

Electrolyte and lithium meshes are assumed to be under contact once the distance (d) between the two meshes become less than the 2.5% of the amplitude (H) of the dendritic protrusion $(d<0.025H)$. After contact, a virtual spring with extremely large magnitude of axial and shear stiffness has been placed between the lithium and electrolyte mesh to prevent further deformation with respect to each other. Under externally applied load, both the meshes move together. Downward movement of the electrolyte has been modeled as a displacement prescribed incremental phenomenon. Under small strain small displacement assumption, the incremental stress has been simply added to the stress obtained at the end of the previous equilibrium step, $\underset{\approx}{\sigma}^{n+1}=\underset{\approx}{\sigma}^{n}+\Delta\underset{\approx}{\sigma}$.

Similar to *pre-stressed* scenario A, a periodic boundary condition has been applied on the left and right boundaries in *relaxed* scenario B as well.

Current density (i_{BV}) due to the electrochemical reaction at the lithium-electrolyte interface is given by the Butler-Volmer equation[37]:

$$i_{BV}=i_{0,ref}\exp\left(\frac{\Delta\mu_{e^-}}{2RT}\right)\left[\exp\left(\frac{F\eta}{2RT}\right)-\exp\left(-\frac{F\eta}{2RT}\right)\right] \tag{8}$$

Here, $i_{0,ref}$ is the reference exchange current density, which is also a function of the local electrolyte concentration. In the present context, extremely low applied current density leads to almost uniform distribution of lithium ions within the electrolyte. Hence, $i_{0,ref}$ can be considered constant throughout the lithium-electrolyte interface. Change in electrochemical potential due to the evolution of mechanical stress has been denoted by the term $\Delta\mu_{e^-}$. The other terms have their usual meaning, which has also been provided in the List of Symbols. Detailed expression of the change in electrochemical potential term $\left(\Delta\mu_{e^-}\right)$ can be given as [36, 37]:

$$\begin{aligned}\Delta\mu_{e^-}\left(x\right) = &-\frac{1}{2}\left(\bar{V}_{Li}+\left(1-t_{Li^+}\right)\bar{V}_{Elec}\right)\cdot \\ &\cdot\left\{-\gamma\kappa+\vec{n}\bullet\left[\vec{n}\bullet\left(\Delta\underset{\approx}{\tau}^{Lithium}-\Delta\underset{\approx}{\tau}^{Electrolyte}\right)\right]\right\}+ \\ &+\frac{1}{2}\left(\bar{V}_{Li}-\left(1-t_{Li^+}\right)\bar{V}_{Elec}\right)\cdot\left(\Delta p^{Lithium}+\Delta p^{Electrolyte}\right)\end{aligned} \tag{9}$$

Here, $\bar{V}_{Li}$ and $\bar{V}_{Elec}$ represents the partial molar volume of lithium and electrolyte salt, respectively, t_{Li^+} is the transference number of the lithium cation $\left(Li^+\right)$ within the electrolyte, γ is the surface energy, κ is the local curvature and $\vec{n}$ represents the normal

vector at the lithium-electrolyte interface. The pressure term is estimated as $\Delta p^{Lithium} = -\sigma_{kk}^{Lithium}/3$ and $\Delta p^{Electrolyte} = -\sigma_{kk}^{Electrolyte}/3$, whereas, the deviatoric stress term is evaluated as $\Delta\tau_{ij}^{Lithium} = -s_{ij}^{Lithium}$ and $\Delta\tau_{ij}^{Electrolyte} = -s_{ij}^{Electrolyte}$. In the 2D computational domain, the local curvature κ has been calculated in a piece-wise fashion according to the following formula[39]:

$$\kappa(x) = \frac{\partial^2 z}{\partial x^2} \times \left[1 + \left(\frac{\partial z}{\partial x}\right)^2\right]^{-3/2} \tag{10}$$

Where, $z(x)$ represents the vertical coordinates of the lithium-electrolyte interface. Since a fixed interfacial displacement is applied in scenario A (*pre-stressed*) as a boundary condition, the curvature does not depend on the elastic modulus of either the lithium electrode or the electrolyte. On the contrary, in scenario B, since the electrolyte is pushed on top of the lithium metal, local curvature of the dendritic protrusion can change significantly. Higher elastic modulus of the electrolyte leads to more flat protrusions.

During operation under relatively low current densities, to estimate whether dendritic protrusions will propagate or not, an effective exchange current density $\left(i_{0,eff}\right)$ has been defined:

$$i_{0,eff}(x) = i_{0,ref} \exp\left(\frac{\Delta\mu_{e^-}(x)}{2RT}\right) \quad (11)$$

If the effective exchange current density at the peak of the protrusion is greater than that at the valley $\left(i_{0,eff,peak} > i_{0,eff,valley}\right)$, dendrites can grow. Otherwise, under the condition that the valley experiences higher effective exchange current density than the peak $\left(i_{0,eff,peak} < i_{0,eff,valley}\right)$, relatively flat lithium deposits would form. Here, propensity of dendrite growth will be analyzed based on the ratio of current density at the peak and the valley.

Results and discussion

Most of the mechanical (such as, elastic modulus, Poisson's ratio) and transport parameters (such as, transference number $\left(t_{Li^+}\right)$, reference exchange current density $\left(i_{0,ref}\right)$) used to run the simulations have been adopted from existing literatures and listed in Table I. It should be noted that only stress evolution has been estimated here, and no transport equations were solved. During operation under low current densities, probability of dendrite formation as predicted by the two different scenarios (*i.e. pre-*

stressed and *relaxed*) would be analyzed here in terms of the effective exchange current density (defined in Eq. (11)). Since extremely low current densities are being considered, the concentration of lithium ions within the electrolyte can be assumed to be same at every point along the lithium-electrolyte interface. Variation in effective exchange current density along the interface comes from two different components (see Eq. (9)):

1. Changes in hydrostatic and deviatoric stress distribution along the lithium-electrolyte interface.
2. Differences in the local surface curvature along the interfacial direction.

Hence, evolution of the stress components and the electrochemical potential term $\left(\Delta\mu_{e^-}\right)$ along the x-direction will be reported next. Different types of electrolyte have been characterized by varying the shear modulus. A fixed value of Poisson's ratio has been assumed for the electrolyte in all the simulations conducted here. Since, the main aim of this study is to elucidate the difference between the two scenarios, exactly same mechanical properties were used while simulating the *pre-stressed* and the *relaxed* case. The deformed configuration of the lithium-electrolyte mesh for the initially *pre-stressed* and *relaxed* scenario is shown schematically in Figure 2(b) and 2(d), respectively. For the *pre-stressed* lithium, surface curvature is independent of electrolyte shear modulus, which is not true for initially *relaxed* lithium.

For the *pre-stressed* lithium (scenario A), variation in effective hydrostatic stress along the interfacial direction is plotted in Figure 3(a) for different values of the electrolyte shear modulus. Even though the dendritic peak is located at $\left(x/L_x\right)\approx 0.5$, the effective hydrostatic stress is tensile at that point for electrolytes with shear modulus

lower than that of lithium metal $\left(G^{Elec} \le G^{Li}\right)$. However, the trend flips and compressive effective hydrostatic stress occurs at the dendrite tip for more stiff electrolytes with shear modulus twice that of lithium metal $\left(G^{Elec} \ge 2G^{Li}\right)$. Occurrence of tensile effective hydrostatic stress at the protrusion peak is due to the tension generated within lithium metal while applying the initial interfacial displacement. For electrolytes with shear modulus higher than that of lithium, the magnitude of the compressive hydrostatic stress within electrolyte exceeds the magnitude of tensile hydrostatic stress that develops within lithium. Hence, the effective hydrostatic stress term becomes positive at the peak.

According to the *pre-stressed* scenario, variation in the effective deviatoric stress along the interface has been demonstrated in Figure 3(b). Irrespective of the electrolyte modulus, its contribution to the electrochemical potential $\left(\Delta\mu_{e^-}\right)$ at the peak of the dendrite is always negative. However, the magnitude of the effective deviatoric stress is much smaller than its hydrostatic counterpart. For extremely low modulus of the electrolyte, the deviatoric stress term negligibly contributes to the electrochemical potential.

Change in the stress and surface curvature induced electrochemical potential along the lithium-electrolyte interface has been demonstrated in Figure 3(c). The $\Delta\mu_{e^-}$

term has been divided by the amplitude of interfacial displacement (H) to ensure that the magnitude of the electrochemical potential is comparable to that reported by Monroe and Newman (see Figure 5 in Ref. [37]). The results clearly indicate that electrochemical potential is positive at the dendrite peak for low modulus electrolytes. However, for electrolytes with shear modulus more than two times in magnitude than that of lithium $\left(G^{Elec} \geq 2G^{Li}\right)$, produce negative electrochemical potential at the peak. Since, the *pre-stressed* scenario has already been analyzed by Monroe and Newman, the results presented in Figure 3(a-c) is exactly same as that reported by them[37]. Direct comparison between Figure 3(c) and 3(a) clearly indicates that the electrochemical potential is significantly governed by the effective hydrostatic stress term. The surface tension (γ) has very small contribution to the overall electrochemical potential for *pre-stressed* lithium.

Next, the initially *relaxed* lithium (scenario B) will be analyzed. Figure 4(a) indicates that the effective hydrostatic stress experienced by initially *relaxed* lithium is mostly compressive all along the lithium-electrolyte interface. Since no pre-existing stress is assumed within the lithium metal, and the electrolyte is pushed on top of the electrode, compressive stresses develop on both the lithium and the electrolyte. The electrolyte has to deform to take the shape of the lithium metal with a dendritic protrusion. Hence, tensile hydrostatic stress of very small magnitude is observed close to the valley where the electrolyte gets pulled along the x-direction. Another important point

to be noted is that the magnitude of effective hydrostatic stress decreases significantly as the shear modulus of the electrolyte drops (this is in contrast to that observed under *pre-stressed* scenario). In other words, materials with lower elastic modulus can deform easily. Therefore, when pushed from the top, electrolyte with low modulus can deform and take the shape of lithium metal without generating of a large amount of stress.

Variation in the effective deviatoric stress term along the lithium-electrolyte interface has been demonstrated in Figure 4(b). Its contribution is mostly negative all along the interface, and becomes positive close to the valley. However, magnitude of the effective deviatoric stress component is much smaller than its hydrostatic counterpart. Similar to the *pre-stressed* lithium, electrolytes with small elastic modulus contribute very little to the electrochemical potential term for initially *relaxed* lithium as well. The minor wiggles in the curve are due to the computational technique adopted to keep the lithium and electrolyte in contact under externally applied load.

Finally, the change in electrochemical potential experienced by the initially *relaxed* lithium due to stress evolution has been reported in Figure 4(c). To make direct comparison with the *pre-stressed* scenario, the electrochemical potential term has been divided by the amplitude of the dendritic protrusion. Comparison between Figure 3(c) and 4(c) indicates that for the case of initially *relaxed* lithium, change in electrochemical potential is negative all along the lithium-electrolyte interface. This is a significant difference between the *pre-stressed* and the *relaxed* scenario. For electrolytes with high shear modulus, the effective electrochemical potential term at the dendrite peak is twice as negative for the initially *relaxed* lithium as compared to its *pre-stressed* counterpart. In the *pre-stressed* scenario, electrolytes with high shear modulus can deform the shape of

the dendritic protrusion and hence affect its curvature significantly when pushed from the top. This correlates very well with Figure 1(e), where the shape of the dendritic protrusion significantly depends on the modulus of the lithium and the electrolyte. Usage of liquid electrolytes (with negligible shear modulus) will lead to very minor change in the shape of the protrusion (and hence the interfacial curvature). Under initially *relaxed* lithium and low modulus of the electrolyte, magnitudes of both effective hydrostatic and deviatoric stress components are so small that majority of the contribution on $\Delta\mu_{e^-}(x)$ come from the surface curvature term $(\kappa\times\gamma)$. For the case of *pre-stressed* lithium, surface curvature does not show any significant impact on electrochemical potential because of its relatively small magnitude.

This variation in the effective electrochemical potential term $(\Delta\mu_{e^-}/H)$ leads to a large difference in the effective exchange current density $(i_{0,eff})$ as observed with initially *pre-stressed* (scenario A) and *relaxed* (scenario B) lithium. Distribution of effective exchange current density along the lithium-electrolyte interface (as a function of *x* location) has been plotted in Figure 5(a) and 5(b) for *pre-stressed* and *relaxed* lithium, respectively (see Eq. (11) for the mathematical expression). Since we perform simulations under conditions that are consistent with low-rate operations, electrolyte concentration induced variation within the reference exchange current density can be neglected. The *pre-stressed* scenario reveals that electrolytes with shear modulus lower

than that of lithium metal experience extremely large magnitude of $i_{0,eff}$ at the protrusion peak as compared to the valley. The opposite distribution of effective exchange current density $\left(i_{0,eff}\right)$ is observed for electrolytes with shear modulus greater than twice that of lithium metal $\left(G^{Elec} \geq 2G^{Li}\right)$. This leads to the conclusion that, under the assumption of *pre-stressed* lithium and soft electrolyte, even at very low current densities, the effective exchange current density at the protrusion peak is much larger than that observed at the valley.

Figure 5(b) demonstrates the distribution of exchange current density along the lithium-electrolyte interface for the case of initially *relaxed* lithium. Irrespective of the electrolyte shear modulus, effective exchange current density at the dendrite peak is smaller in magnitude than that observed at the valley. If the electrolyte modulus is much smaller than that of lithium (also applicable to liquid electrolyte with almost zero shear stiffness), $i_{0,eff}$ at the peak is only half of that at the valley. However, as the modulus of the electrolyte increases, it induces enhanced magnitude of hydrostatic and deviatoric stress on the lithium-electrolyte interface, resulting in variation of $i_{0,eff}(x)$ over multiple orders of magnitude.

For the case of liquid electrolytes characterized by extremely low elastic modulus[40], the effective exchange current density at the valley should be approximately twice than that at the peak of a lithium nucleus (see Figure 5(b)). As a result, according to the scenario of *relaxed* lithium, for operation under low current density with liquid electrolyte, no dendrite growth should occur (which is similar to that observed experimentally) [25]. For polymer electrolytes (such as PEO) where the shear modulus is approximately one order of magnitude smaller than that of Li[41], effective exchange current density is still two-three orders of magnitude higher at the valley than that observed at the peak (see Figure 5(b)). These simulations suggest that during operation at low current densities using polymer electrolyte protection layers, dendrite formation is unlikely, consistent with the experimental observations[42]. However, under high current density operation, dendrite growth has been observed experimentally in PEO based electrolytes[43]. While our present simulation does not address the high current density case because we ignore concentration and ohmic polarization effects, the experimental observations suggest that dendrite formation at high current densities is dominated by the current distribution in the electrolyte.

A major drawback of the present theory and that of Monroe and Newman is that only elastic deformation of lithium and electrolyte has been taken into account, and plasticity has been neglected altogether. Present research indicates that for initially *relaxed* lithium and $G^{Elec} = 10^{-4} G^{Li}$, less than 0.4MPa stress evolves in both lithium and electrolyte. However, under the same conditions but with $G^{Elec} = 10^{-1} G^{Li}$, stresses of magnitude more than 100MPa has been observed in both lithium and electrolyte at the

interface. The yield strength of Li is around 0.8MPa – 1.0MPa[38]. Yield strength for PEO based polymers are approximately 10MPa[44]. Hence, plastic deformation of the lithium electrode and electrolyte is inevitable when stiff electrolytes are used. This is true for both the cases of initially *pre-stressed* and *relaxed* lithium. Plasticity of both lithium metal and electrolyte would not allow the stress to increase to an extremely large magnitude, which is observed in the present context due to elastic deformations. Large tensile and/or compressive stresses lead to orders of magnitude variation in the effective exchange current density (see Figures 5 and 6). Plastic deformation would allow the magnitude of stress, and subsequently the effective exchange current density, to remain within realistic limits. This aspect will be the subject of future research.

During electrochemical deposition of lithium, given the fact that a lithium nucleus evolves, dendrite growth is possible only when the current density at the protrusion peak is greater than the current density at the valley. Figure 6 demonstrates the ratio of exchange current density at the peak over that at the valley $\left(i_{0,eff,peak}/i_{0,eff,valley}\right)$ for both the *pre-stressed* (red circle) and *relaxed* (black square) lithium with respect to electrolyte shear modulus. The blue dashed line indicates the region where both the current densities are equal (value 1.0). If the current density ratio lies below this limit $\left(i_{0,eff,peak}/i_{0,eff,valley} \leq 1\right)$, no dendrite will grow. However, if the ratio between the two

exchange current densities lie above the blue dashed line $\left(i_{0,eff,peak}/i_{0,eff,valley} \geq 1\right)$, dendrite growth cannot be prevented using mechanical means. The effective exchange current density being analyzed here is applicable to operation under low rates of current densities, where the effect of electrolyte concentration can be neglected. The red curve indicates that even during low rates of operation, the *pre-stressed* lithium would lead to severe dendrite growth if the shear modulus of the electrolyte were smaller than that of lithium metal. However, this is usually not observed in experiments for both liquid and polymer electrolytes [9, 42, 45]. Irrespective of the type of electrolyte, dendritic protrusions evolve only during operation at high current densities.

The black curve, which corresponds to the initially *relaxed* lithium, predominantly indicates that dendrite growth can be suppressed by any electrolyte as long as the cell is being operated at low rates (see Figure 6). It has been observed experimentally that $LiPF_6$ in EC/DMC based liquid electrolytes $\left(G^{Elec} \leq 10^{-4} \times G^{Li}\right)$ form dendrite free (mossy) deposits of lithium under low current density operation, and several dendritic protrusions evolve at higher rates of current densities[25]. Similarly, $LiPF_6$ and LiTFSI based polymer electrolytes $\left(G^{Elec} = 10^{-1} \times G^{Li}\right)$ also show mossy lithium deposits at small current densities[9, 42], and dendritic protrusions are observed at large rates close to the limiting current density[9, 43]. These experimental observations are in good agreement with the theoretical predictions made by the black curve in Figure 6.

For the case of initially *relaxed* lithium, electrolytes with small shear modulus $\left(G^{Elec} \le 10^{-3} G^{Li}\right)$ experiences negligible hydrostatic and deviatoric stress on both lithium and electrolyte. Majority of the contribution to the change in electrochemical potential term $\left(\Delta\mu_{e^-}\right)$ comes from surface tension $\left(\gamma\right)$. For very soft electrolytes (*e.g.,* liquid based), surface curvature $\left(\kappa\right)$ of the dendritic protrusion does not change significantly. Hence, the difference in exchange current density at the peak and valley for low modulus electrolyte is due to the stabilizing effect of the negative surface curvature observed at the protrusion peak. Under the condition of *pre-stressed* lithium, impact of surface curvature is always negligible[37].

In the present context, it should also be mentioned that only small-strain/small-displacement analysis has been conducted here. The main focus here has been to analyze the distribution of effective exchange current density after the formation of a lithium nucleus during electro-deposition at very low rates of current densities. Since the size of the lithium protrusion is not large, the linear elasticity theory can still be applicable. However, while modeling the growth of dendritic protrusions, large deformation theories must be taken into account.

Conclusion

A finite-element-method-based computational technique has been developed that can estimate the evolution of hydrostatic and deviatoric stress around a dendritic protrusion. Under low rates of operating current densities, the effective exchange current density at the protrusion peak with respect to the valley dictates the propensity of dendrite formation. Two different scenarios have been considered here: i) Initially *pre-stressed* lithium, and ii) Initially *relaxed* lithium. It has been observed that significant tensile stress acts on the lithium electrode under *pre-stressed* condition, whereas for the initially *relaxed* lithium, compressive stresses act on the electrode, electrolyte and the electrochemically deposited lithium. This variation in stress evolution leads to significant difference in effective exchange current density for the two scenarios of *pre-stressed* and *relaxed* lithium (see Figure 6).

If the shear modulus of the electrolyte is less than that of the lithium metal, severe dendrite growth should occur on initially *pre-stressed* lithium. According to the *pre-stressed* scenario, suppression of dendrite growth is only possible if the elastic modulus of the electrolyte is two times larger than that of lithium. The initially *relaxed* lithium leads to suppression of dendrites under low rates of operating current densities. This behavior is independent of the electrolyte shear modulus. Predictions made by the *relaxed* scenario are consistent with previous experimental reports. For electrolytes with shear modulus similar in magnitude as that of lithium metal, the *relaxed* scenario leads to multiple orders of magnitude higher effective exchange current densities at the valley as compared to the protrusion peak. In the present analysis, only elastic deformation of lithium has been taken into consideration. Plastic deformation of both lithium electrode and polymer electrolyte is possible. That can lead to significantly different effective

exchange current density for both the *pre-stressed* and *relaxed* scenario. Elucidation of proper stress evolution during lithium nucleation can help to devise new and effective techniques to prevent dendrite growth.

Although there is no experimental data presently available for quantitative validation of this model, the finding that initially relaxed lithium sees no dendrite formation at small applied current densities is consistent with typical experimental observations. For quantitative validation, a non-invasive *in situ* technique such as X-ray nanotomography using a specially-designed cell might allow the direct observation of the very early growth of a lithium protrusion, the scenario considered in this work.

The present work has focused on the effect of variation in mechanical stress between the peak and valley of the dendritic protrusion, under operation at lower current densities and at relatively high temperatures. These conditions lead to uniform distributions of concentration and potential between the peak and valley of the dendritic protrusion, making the corresponding impact on reaction current density negligible. While the effects of current density and temperature on the overall dendrite growth process have not been considered in the present context, one can predict these qualitatively. In general, operation at higher current density would lead to concentration and potential gradients between the peak and valley of the dendritic protrusion, which in turn would lead to higher reaction current and enhanced deposition of lithium at the protrusion peak, thereby promoting dendrite growth. Electrolyte conductivity and diffusivity typically decrease significantly with decreasing temperature. Hence, the propensity of dendrites to grow increases significantly during operation at lower ambient temperatures. To incorporate the effects of current density and local temperature on the

overall dendrite formation procedure would require significant additional computational effort. These will be addressed as a part of a future study.

The major conclusions from the present study have been provided below:

1. The concept of initially *pre-stressed* lithium gives rise to growth of dendritic protrusions for low modulus electrolytes. Initially *relaxed* lithium leads to more realistic predictions of dendrite growth.
2. Growth of dendrites is dominated by the current distribution in the electrolyte. Application of mechanical forces has the potential to mitigate dendritic protrusions.
3. Elasto-plastic deformation of the lithium electrode and the electrolyte (if possible) is inevitable. Hence, assuming elastic deformation of the lithium/electrolyte leads to unrealistic magnitudes of stress. Plasticity of lithium and/or electrolyte must be incorporated within the computational model to estimate the correct magnitude of stress evolution, and subsequently the effective exchange current density.

Acknowledgements

This work was supported by the Assistant Secretary for Energy Efficiency and Renewable Energy, Office of Vehicle Technologies of the U.S. Department of Energy under Contract No. DE-AC02-05CH11231 under the Battery Materials Research (BMR) Program.

Appendix

The small strain small displacement finite element procedure adopted to solve the mechanical equilibrium equation (see Eq. (2)). Details of the solution procedure will be

reported here. The domain has been discretized into multiple elements where the equilibrium equation has been solved in an effective fashion through the evaluation of the weak form[46]. The quasistatic momentum balance equation has been multiplied with a kinematically admissible weight function $\left(\vec{\phi}\right)$, and integrated over an element $\left(\Omega_e\right)$:

$$\int_{\Omega_e}\left(\vec{\nabla}\bullet\underset{\approx}{\sigma}\right)\bullet\vec{\phi}\,d\Omega=0 \tag{A1}$$

Integration by parts gives:

$$\int_{\Omega_e}\left(\vec{\nabla}\bullet\left(\underset{\approx}{\sigma}\bullet\vec{\phi}\right)-\underset{\approx}{\sigma}:\left(\vec{\nabla}\otimes\vec{\phi}\right)\right)d\Omega=0 \tag{A2}$$

Assuming that $\vec{n}$ indicates outer normal vector, applying the divergence theorem gives:

$$\int_{\Gamma_e}\left(\vec{n}\bullet\underset{\approx}{\sigma}\right)\bullet\vec{\phi}\,d\Gamma-\int_{\Omega_e}\left(\vec{\nabla}\otimes\vec{\phi}\right):\underset{\approx}{\sigma}d\Omega=0 \tag{A3}$$

Here, Γ_e indicates the domain boundary. Using the stress-strain constitutive relations $\left(\underset{\approx}{\sigma}=\underset{\approx}{C}:\underset{\approx}{\epsilon}\right)$:

$$\int_{\Gamma_e}\vec{t}\bullet\vec{\phi}\,d\Gamma-\int_{\Omega_e}\left(\vec{\nabla}\otimes\vec{\phi}\right):\underset{\approx}{C}:\underset{\approx}{\epsilon}d\Omega=0 \tag{A4}$$

Here, $\vec{t}$ is the traction vector, and its value at the boundary indicates the boundary condition. Due to the inherent symmetry of the strain tensor, $\underset{\approx}{\epsilon} = \vec{\nabla} \otimes \vec{u}$, where $\vec{u}$ is the displacement vector. Writing all the variables using shape functions $\left(N_{ij}\right)$ and the B matrix (where, $B_{ij} = D_{ik} N_{kj}$),

$$\int_{\Omega_e} \vec{\phi}^T B^T : \underset{\approx}{C} : B\vec{u}\, d\Omega = \int_{\Gamma_e} \vec{\phi}^T N^T \bullet \vec{t}\, d\Gamma \tag{A5}$$

As this must hold for all the test functions, it is possible to conclude:

$$\left[K\right]\left\{u\right\} = \left\{f\right\} \tag{A6}$$

Where $\left[K\right]$ is the stiffness matrix and $\left\{f\right\}$ stands for the externally applied force, which is also used as the right hand side vector for this particular simulation. This gives a brief overview of how the mechanical equilibrium equation has been solved using the finite element method. For more details, see, for instance, [46, 47].

List of symbols

Roman

$\underset{\approx}{s}, s_{ij}$ deviatoric stress tensor

$\vec{u}, u_i$	displacement vector
$\vec{x}, x_i$	position vector
G	shear modulus
H	amplitude
d	distance between lithium electrode and electrolyte
i_{BV}	Butler-Volmer current density
$i_{0,ref}$	reference exchange current density
R	universal gas constant
T	temperature
F	Faraday's constant
$\bar{V}_{Li}$	partial molar volume of lithium metal
$\bar{V}_{Elec}$	partial molar volume of electrolyte salt
t_{Li}	lithium ion transference number
Δp	hydrostatic pressure
z	vertical coordinate

$i_{0,eff}$ effective exchange current density

L_x length of computational domain along the x-direction

$\underset{\approx}{C}$ constitutive tensor

$\vec{t}$ traction vector

N_{ij} shape function matrix

D_{ij} matrix of derivatives

B_{ij} differential operated on the shape function

$\left[K\right]$ global stiffness matrix

$\left\{u\right\}$ global displacement vector

$\left\{f\right\}$ global force vector

Greek

$\vec{\nabla}$ gradient operator

$\underset{\approx}{\sigma}, \sigma_{ij}$ stress tensor

σ_{kk} hydrostatic stress

δ_{ij}	Kronecker delta function
$\underset{\approx}{\epsilon}, \epsilon_{ij}$	stress tensor
ν	Poisson's ratio
ω	frequency
$\Delta\underset{\approx}{\sigma}$	stress increment
$\Delta\mu_{e^-}$	change in electrochemical potential due to stress evolution
η	overpotential
γ	surface energy
κ	surface curvature
$\Delta\underset{\approx}{\tau}$	deviatoric stress tensor
$\vec{\phi}$	weight function
Ω_e	domain of a finite element
Γ_e	domain boundary

References

1. Besenhard, J.O. and G. Eichinger, *High-Energy Density Lithium Cells .1. Electrolytes and Anodes.* Journal of Electroanalytical Chemistry, 1976. **68**(1): p. 1-18.
2. Eichinger, G. and J.O. Besenhard, *High-Energy Density Lithium Cells .2. Cathodes and Complete Cells.* Journal of Electroanalytical Chemistry, 1976. **72**(1): p. 1-31.
3. Dunning, J.S., et al., *A Secondary, Nonaqueous Solvent Battery* Journal of the Electrochemical Society, 1971. **118**: p. 1886.
4. Monroe, C. and J. Newman, *Dendrite growth in lithium/polymer systems - A propagation model for liquid electrolytes under galvanostatic conditions.* Journal of the Electrochemical Society, 2003. **150**(10): p. A1377-A1384.
5. Xu, W., et al., *Lithium metal anodes for rechargeable batteries.* Energy & Environmental Science, 2014. **7**(2): p. 513-537.
6. Aurbach, D. and Y. Cohen, *The application of atomic force microscopy for the study of Li deposition processes.* Journal of the Electrochemical Society, 1996. **143**(11): p. 3525-3532.
7. Selim, R. and P. Bro, *Some Observations on Recchargeable Lithium Electrodes in a Propylene Carbonate Electrolyte.* Journal of the Electrochemical Society, 1974. **121**: p. 1457.
8. Yamaki, J., et al., *A consideration of the morphology of electrochemically deposited lithium in an organic electrolyte.* Journal of Power Sources, 1998. **74**(2): p. 219-227.
9. Orsini, F., et al., *In situ SEM study of the interfaces in plastic lithium cells.* Journal of Power Sources, 1999. **81**: p. 918-921.
10. Li, Z., et al., *A review of lithium deposition in lithium-ion and lithium metal secondary batteries.* Journal of Power Sources, 2014. **254**: p. 168-182.
11. Dolle, M., et al., *Live scanning electron microscope observations of dendritic growth in lithium/polymer cells.* Electrochemical and Solid State Letters, 2002. **5**(12): p. A286-A289.
12. Ghassemi, H., et al., *Real-time observation of lithium fibers growth inside a nanoscale lithium-ion battery.* Applied Physics Letters, 2011. **99**(12).
13. Stark, J.K., Y. Ding, and P.A. Kohl, *Nucleation of Electrodeposited Lithium Metal: Dendritic Growth and the Effect of Co-Deposited Sodium.* Journal of the Electrochemical Society, 2013. **160**(9): p. D337-D342.
14. Tang, C.-Y. and S.J. Dillon, *In Situ Scanning Electron Microscopy Characterization of the Mechanism for Li Dendrite Growth.* Journal of the Electrochemical Society, 2016. **163**(8): p. A1660 - A1665.
15. Schweikert, N., et al., *Suppressed lithium dendrite growth in lithium batteries using ionic liquid electrolytes: Investigation by electrochemical impedance spectroscopy, scanning electron microscopy, and in situ Li-7 nuclear magnetic resonance spectroscopy.* Journal of Power Sources, 2013. **228**: p. 237-243.
16. Umeda, G.A., et al., *Protection of lithium metal surfaces using tetraethoxysilane.* Journal of Materials Chemistry, 2011. **21**(5): p. 1593-1599.
17. Chang, H.J., et al., *Correlating Microstructural Lithium Metal Growth with Electrolyte Salt Depletion in Lithium Batteries Using Li-7 MRI.* Journal of the American Chemical Society, 2015. **137**(48): p. 15209-15216.

18. Cheng, X.B., et al., *A Review of Solid Electrolyte Interphases on Lithium Metal Anode.* Advanced Science, 2016. **3**(3).
19. Takehara, Z., *Future prospects of the lithium metal anode.* Journal of Power Sources, 1997. **68**(1): p. 82-86.
20. Li, W.Y., et al., *The synergetic effect of lithium polysulfide and lithium nitrate to prevent lithium dendrite growth.* Nature Communications, 2015. **6**.
21. Cohen, Y.S., Y. Cohen, and D. Aurbach, *Micromorphological studies of lithium electrodes in alkyl carbonate solutions using in situ atomic force microscopy.* Journal of Physical Chemistry B, 2000. **104**(51): p. 12282-12291.
22. Shin, W.K., A.G. Kannan, and D.W. Kim, *Effective Suppression of Dendritic Lithium Growth Using an Ultrathin Coating of Nitrogen and Sulfur Codoped Graphene Nanosheets on Polymer Separator for Lithium Metal Batteries.* Acs Applied Materials & Interfaces, 2015. **7**(42): p. 23700-23707.
23. Peng, Z., et al., *Volumetric variation confinement: surface protective structure for high cyclic stability of lithium metal electrodes.* Journal of Materials Chemistry A, 2016. **4**(7): p. 2427-2432.
24. Khurana, R., et al., *Suppression of Lithium Dendrite Growth Using Cross-Linked Polyethylene/Poly(ethylene oxide) Electrolytes: A New Approach for Practical Lithium-Metal Polymer Batteries.* Journal of the American Chemical Society, 2014. **136**(20): p. 7395-7402.
25. Chang, H.J., et al., *Investigating Li Microstructure Formation on Li Anodes for Lithium Batteries by in Situ Li-6/Li-7 NMR and SEM.* Journal of Physical Chemistry C, 2015. **119**(29): p. 16443-16451.
26. Gireaud, L., et al., *Lithium metal stripping/plating mechanisms studies: A metallurgical approach.* Electrochemistry Communications, 2006. **8**(10): p. 1639-1649.
27. Barton, J.L. and J.O.M. Bockris, *The electrolytic growth of dendrites from ionic solutions.* Proceedings of the Royal Society of London. Series: A. , 1962. **268**: p. 485 - 505.
28. Diggle, J.W., A.R. Despic, and J.O.M. Bockris, *The Mechanism of the Dendritic Electrocrystallization of Zinc.* Journal of the Electrochemical Society, 1969. **116**(11): p. 1503 - 1514.
29. Brissot, C., et al., *Dendritic growth mechanisms in lithium/polymer cells.* Journal of Power Sources, 1999. **81**: p. 925-929.
30. Chazalviel, J.N., *Electrochemical Aspects of the Generation of Ramified Metallic Electrodeposits.* Physical Review A, 1990. **42**(12): p. 7355-7367.
31. Ely, D.R. and R.E. Garcia, *Heterogeneous Nucleation and Growth of Lithium Electrodeposits on Negative Electrodes.* Journal of the Electrochemical Society, 2013. **160**(4): p. A662-A668.
32. Jana, A., D.R. Ely, and R.E. Garcia, *Dendrite-separator interactions in lithium-based batteries.* Journal of Power Sources, 2015. **275**: p. 912-921.
33. Chen, L., et al., *Modulation of dendritic patterns during electrodeposition: A nonlinear phase-field model.* Journal of Power Sources, 2015. **300**: p. 376-385.
34. Cogswell, D.A., *Quantitative phase-field modeling of dendritic electrodeposition.* Physical Review E, 2015. **92**(1).

35. Aryanfar, A., et al., *Dynamics of Lithium Dendrite Growth and Inhibition: Pulse Charging Experiments and Monte Carlo Calculations.* Journal of Physical Chemistry Letters, 2014. **5**(10): p. 1721-1726.
36. Monroe, C. and J. Newman, *The effect of interfacial deformation on electrodeposition kinetics.* Journal of the Electrochemical Society, 2004. **151**(6): p. A880-A886.
37. Monroe, C. and J. Newman, *The impact of elastic deformation on deposition kinetics at lithium/polymer interfaces.* Journal of the Electrochemical Society, 2005. **152**(2): p. A396-A404.
38. Schultz, R., *Lithium: Measurement of Young's Modulus and Yield Strength.* Fermilab-TM-2191, 2002: p. 1 - 6.
39. Deen, W.M., *Analysis of Transport Phenomena*. 1998, New York: Oxford University Press.
40. Schaefer, J.L., et al., *Electrolytes for high-energy lithium batteries.* Applied Nanoscience, 2012. **2**: p. 91 - 109.
41. Moreno, M., et al., *Electrical and mechanical properties of poly(ethylene oxide)/intercalated clay polymer electrolyte.* Electrochimica Acta, 2011. **58**: p. 112-118.
42. Porcarelli, L., et al., *Super Soft All-Ethylene Oxide Polymer Electrolyte for Safe All-Solid Lithium Batteries.* Scientific Reports, 2016. **6**.
43. Harry, K.J., D.Y. Parkinson, and N.P. Balsara, *Failure Analysis of Batteries Using Synchrotron-based Hard X-ray Microtomography.* Jove-Journal of Visualized Experiments, 2015(102).
44. Husken, D. and R.J. Gaymans, *The tensile properties of poly(ethylene oxide)-based segmented block copolymers in the dry and wet state.* Journal of Materials Science, 2009. **44**(10): p. 2656-2664.
45. Zhang, R., et al., *Conductive Nanostructured Scaffolds Render Low Local Current Density to Inhibit Lithium Dendrite Growth.* Advanced Materials, 2016. **28**(11): p. 2155-2162.
46. Reddy, J.N., *An Introduction to the Finite Element Method*. 2003, New Delhi: Tata McGraw-Hill Publishing Company Limited.
47. Cook, R.D., et al., *Concenpts and Applications of Finite Element Analysis*. 2000, Singapore: John Wiley and Sons (Asia) Pte. Ltd.

List of tables

Table: I. A list of the parameters used in the present simulation is provided below along with the references from where they have been adopted.

List of figures

Figure: 6. Ratio of the effective exchange current density observed at the peak and the valley is plotted with respect to the ratio between electrolytes over lithium shear modulus. If the current density in the peak is greater than the current density in the valley, the dendrite will grow. Otherwise, growth of the dendritic protrusion will not occur. Hence, it is preferable to have the ratio of current density at the peak over current density at the valley to be less than 1.0. The scenario with initially *relaxed* lithium indicates that for electrolyte with any modulus shows the tendency to prevent dendrite growth. On the contrary, *pre-stressed* lithium indicates that dendrite growth should automatically occur for the case of low modulus electrolytes, irrespective of the applied current density (which is not usually observed in the real world).

Table: I. A list of the parameters used in the present simulation is provided below along with the references from where they have been adopted.

Name	Symbol	Unit	Value	References
Surface energy	γ	J/m^2	1.716	[37]
Lithium shear modulus	G^{Li}	GPa	3.4	[37]
Lithium Poisson's ratio	ν^{Li}	--	0.42	[37]
Electrolyte Poisson's ratio	ν^{Elec}	--	0.3	[37]
Partial molar volume of lithium	$\bar{V}_{Li}$	m^3/mol	$1.3\text{x}10^{-5}$	[37]
Partial molar volume of electrolyte salt	$\bar{V}_{Elec}$	m^3/mol	$1.674\text{x}10^{-4}$	[37]
Lithium transference number	t_{Li}	--	0.3	[37]
Frequency	ω	m^{-1}	10^8	[37]
Amplitude	H	nm	4.0	[37]
Reference exchange current density	$i_{0,ref}$	A/m^2	1.0	--
Domain length	L_x	m	$2\pi/\omega$	[37]
Universal gas constant	R	$J/mol-K$	8.314	--
Temperature	T	K	298.15	--

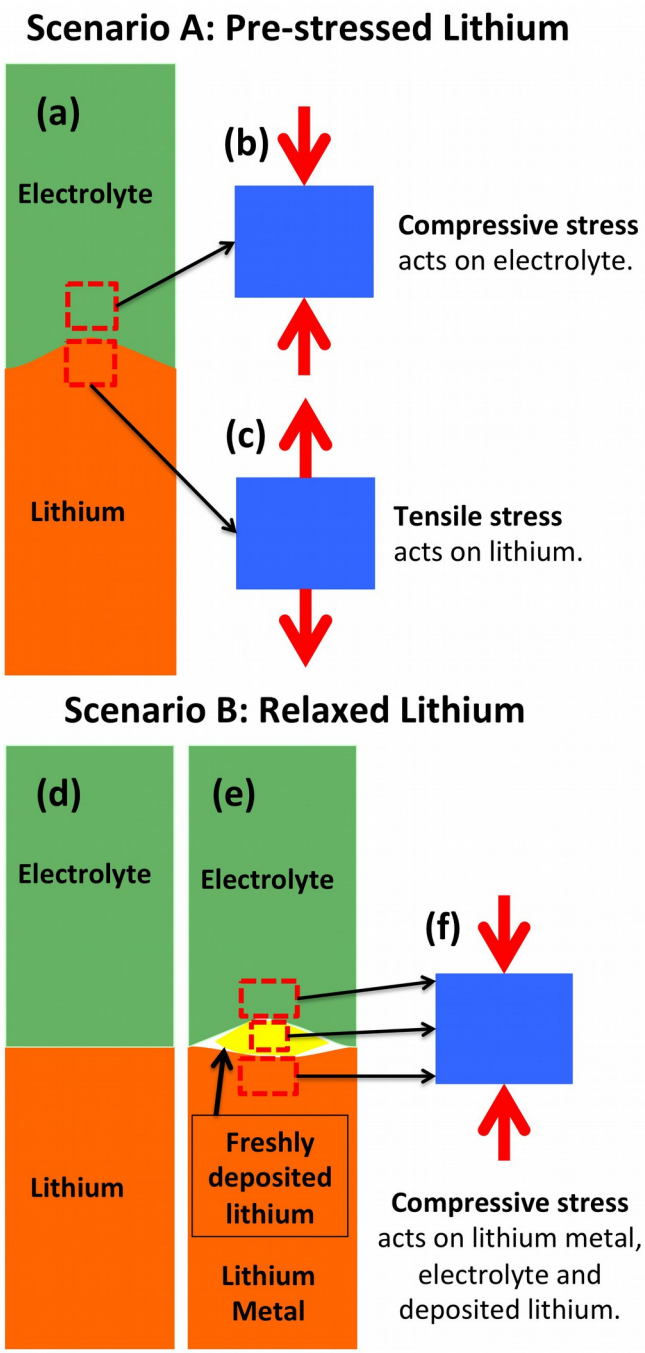

Figure: 1. Schematic representation of two different scenarios observed at the lithium metal – electrolyte interface. Scenario: A. *Pre-stressed* lithium metal (analyzed by Monroe and Newman, *JES* (2005)). Scenario: B. *Relaxed* initial state of lithium metal. (a) Schematic demonstration of *pre-stressed* lithium/electrolyte interface. (b) Compressive stress acting on the electrolyte. (c) Tension acting on top of lithium metal. (d) Schematic representation of the initially *relaxed* lithium/electrolyte interface. (e) Lithium deposition at the lithium/electrolyte interface due to electrochemical reactions. (f) Compressive stress acting on lithium metal, electrolyte and newly deposited lithium.

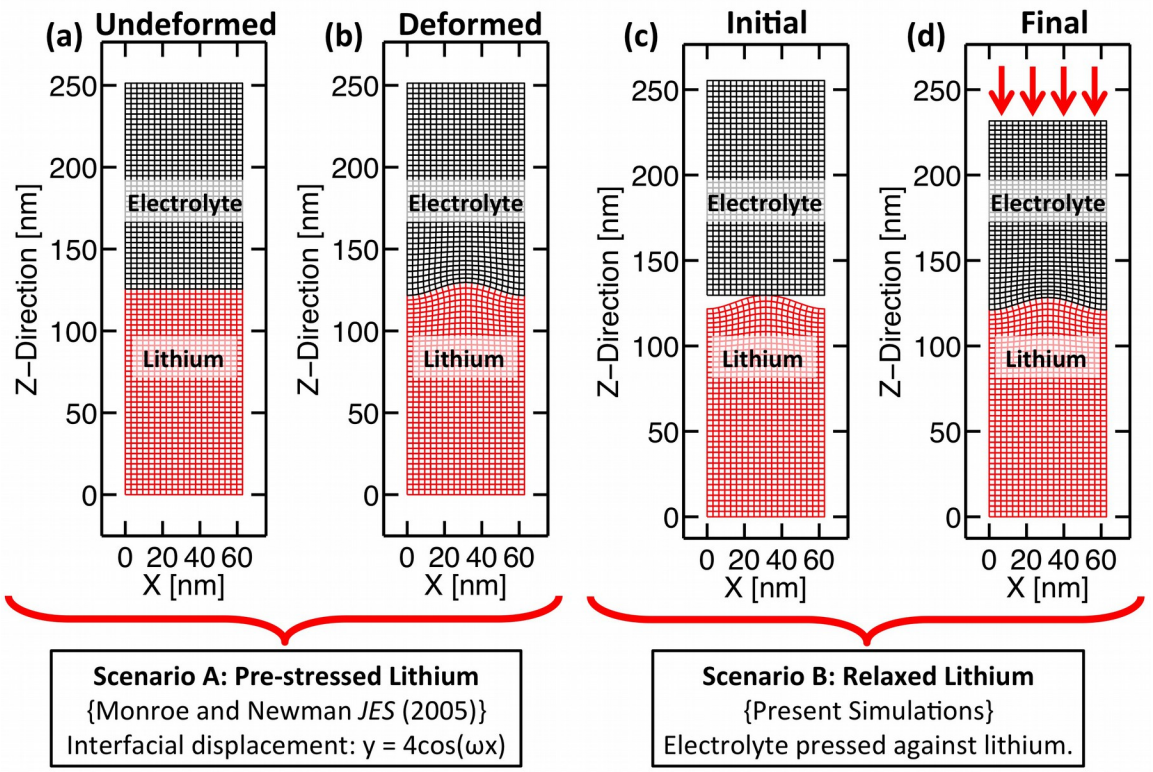

Figure: 2. Computational mesh of the two different scenarios being considered in this study. (a) and (b) demonstrates the *pre-stressed* lithium and electrolyte interface analyzed by Monroe and Newman (JES, 2005). (c) and (d) shows the interaction of the *relaxed* lithium metal with electrolyte as it is pressed on top of the lithium metal. (a) Computational undeformed initial configuration of the lithium and electrolyte, where the interface is flat. (b) Deformed shape of *pre-stressed* lithium (under tension) and electrolyte (under compression). (c) Initial configuration of the *relaxed* scenario, where sinusoidal displacement is applied only on the lithium metal. Electrolyte remains flat and touches the top of lithium metal. (d) Electrolyte is pushed on top of lithium such that it entirely comes in contact with the deformed lithium metal. This induces compressive stress in both lithium and electrolyte.

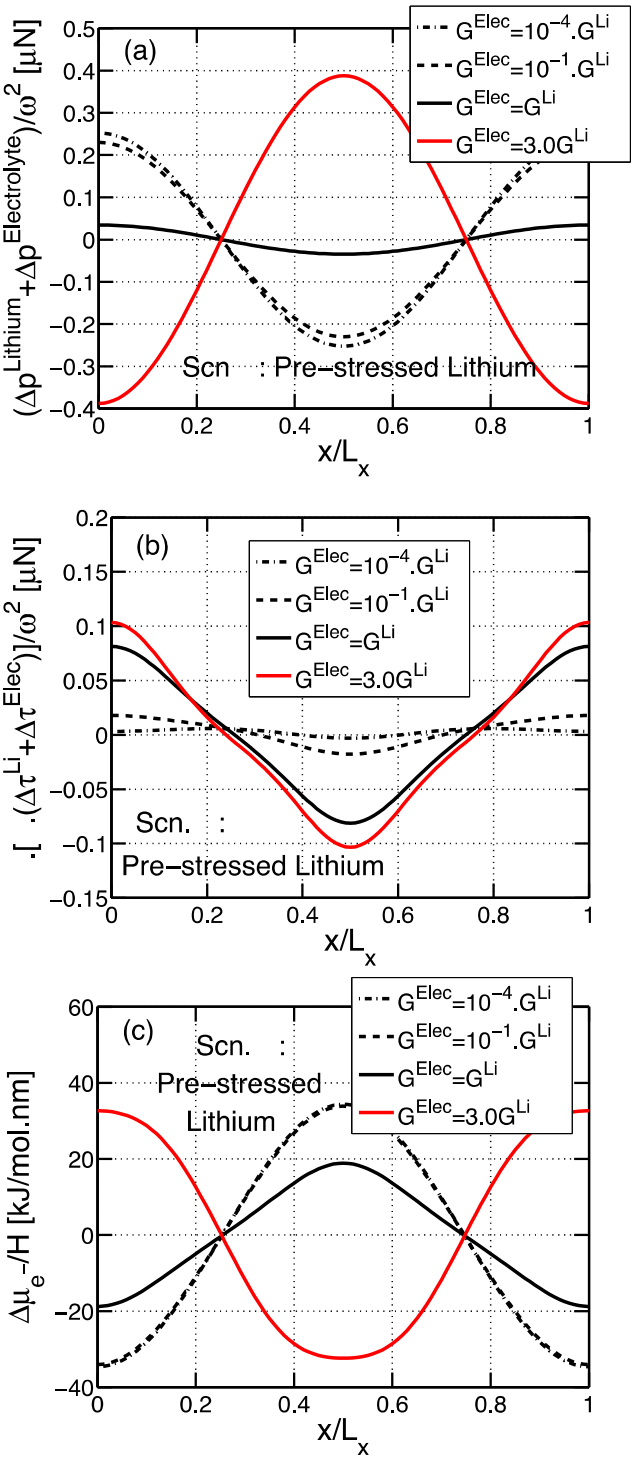

Figure: 3. *Scenario A: Pre-stressed Lithium.* Variation in stress and stress-induced electrochemical potential along the x-direction obtained under the assumption of *pre-stressed* lithium (adopted by Monroe and Newman (*JES*, 2005)). The *peak* is located at the center, and the *valleys* are at the two sides. (a) The effective hydrostatic stress term. (b) The effective deviatoric stress term. (c) Mechanical strain induced electrochemical potential term. The surface energy has little impact on the electrochemical potential term as compared to the hydrostatic and deviatoric stresses. These results are similar to that reported by Monroe and Newman (*JES*, 2005).

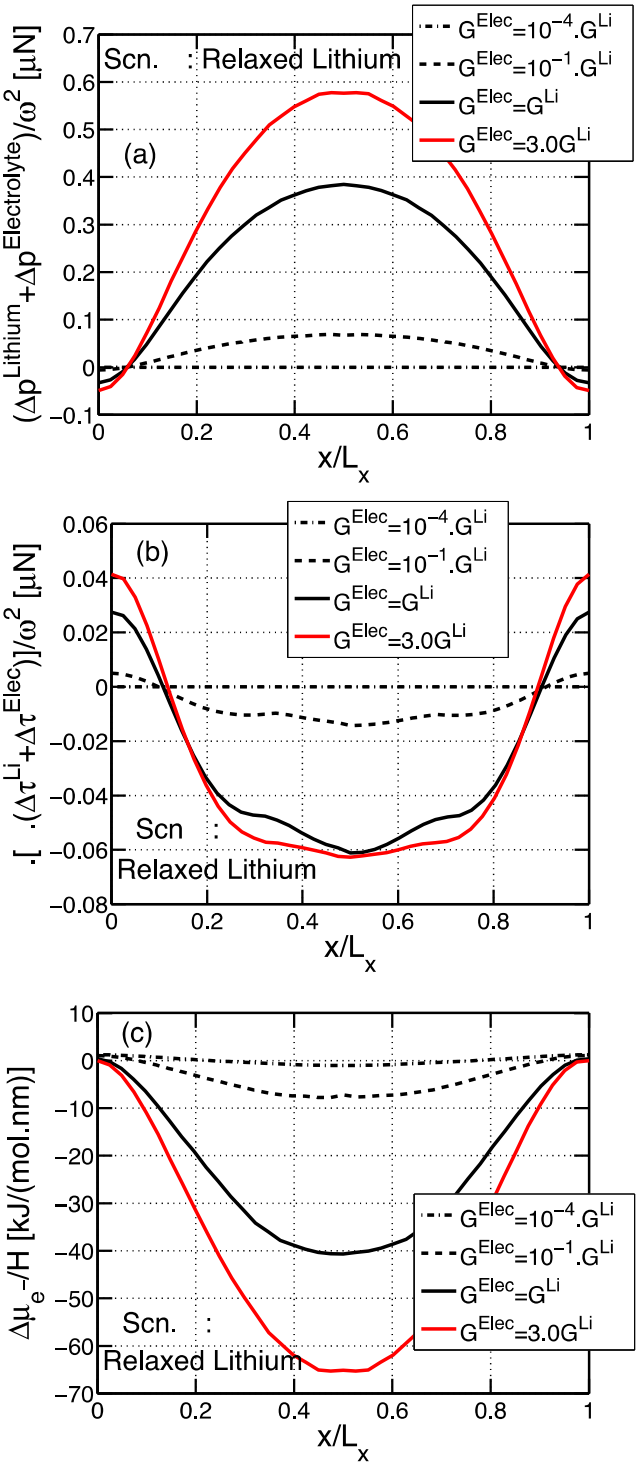

Figure: 4. *Scenario B: Relaxed Lithium.* Variation in stress and electrochemical potential along the x-direction under the condition of initially *relaxed* lithium metal. The *peak* is located at the center, and the *valleys* are at the two sides. (a) Effective hydrostatic stress term remains compressive throughout the length. It becomes tensile extremely close to the valley. (b) Effective deviatoric stress term. (c) Stress induced change in electrochemical potential. The numbers indicate that the system is predominantly under compression, which impedes the growth of dendrites.

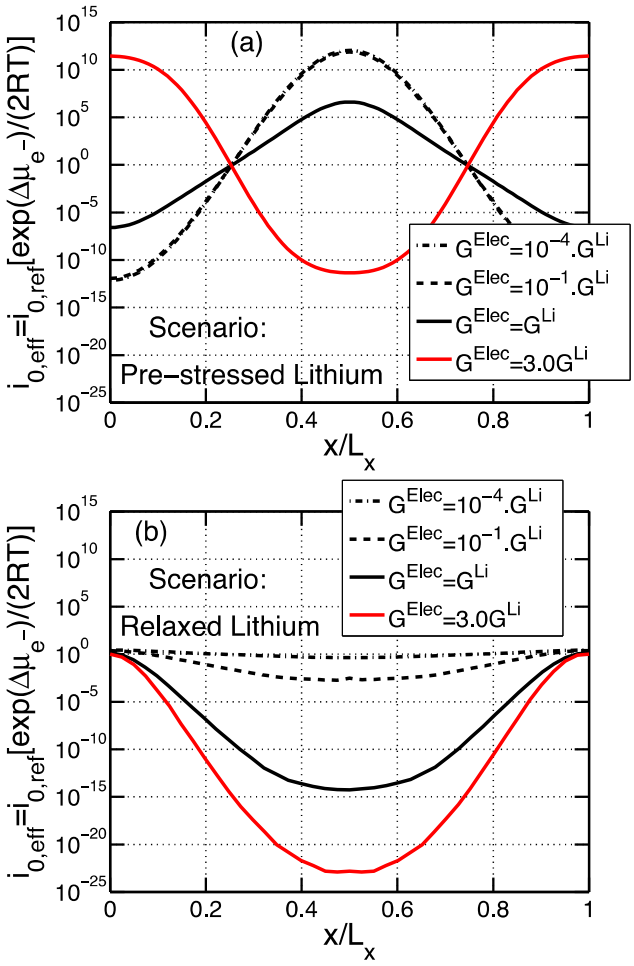

Figure: 5. Effective exchange current density as estimated using Eq. (11). The *peak* is located at the center, and the *valleys* are at the two sides. (a) The *pre-stressed* lithium scenario adopted by Monroe and Newman (JES, 2005). The effective exchange current density varies over several orders of magnitude. (b) The scenario of initially *relaxed* lithium adopted in the present analysis. For very soft electrolyte (such as liquids), the effective exchange current density changes by only a factor of two (may be difficult to conclude just from the figure). However, as the elastic modulus of the electrolyte phase increases, the effective exchange current density at the peak becomes several orders of magnitude smaller than that observed within the valley region.

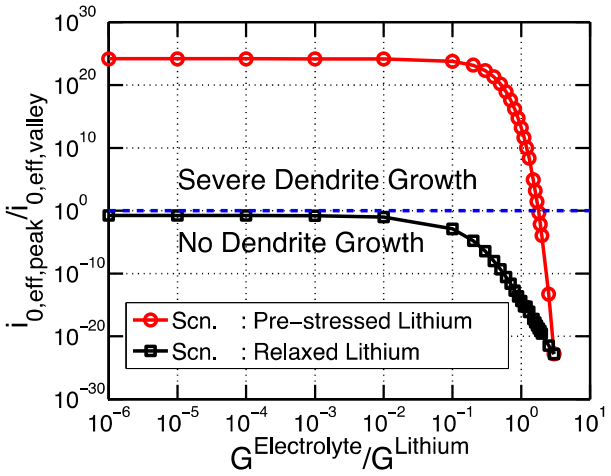

Figure: 6. Ratio of the effective exchange current density observed at the peak and the valley is plotted with respect to the ratio between electrolytes over lithium shear modulus. If the current density in the peak is greater than the current density in the valley, the dendrite will grow. Otherwise, growth of the dendritic protrusion will not occur. Hence, it is preferable to have the ratio of current density at the peak over current density at the valley to be less than 1.0. The scenario with initially *relaxed* lithium indicates that for electrolyte with any modulus shows the tendency to prevent dendrite growth. On the contrary, *pre-stressed* lithium indicates that dendrite growth should automatically occur for the case of low modulus electrolytes, irrespective of the applied current density (which is not usually observed in the real world).